Directional Reflectivity of the Ellipsoid Zone in Dry Age-Related Macular Degeneration

Shane M. Griffin, MCR; Yali Jia, PhD; Alicia J. Johnson, MPH; Bhavna J. Antony, PhD; H. Richard McDonald, MD; Robert N. Johnson, MD, Brandon J. Lujan, MD

BACKGROUND AND OBJECTIVE: Ellipsoid zone (EZ) reflectivity on optical coherence tomography (OCT) is affected by the orientation of the scanning beam. The authors sought to determine how directional reflectivity changes in dry age-related macular degeneration (AMD).

PATIENTS AND METHODS: Retrospective image analysis included 17 control and 20 dry AMD subjects. Directional OCT (D-OCT) was performed using multiple displaced pupil entrance positions. EZ pixel values and apparent incidence angles were measured.

RESULTS: EZ reflectivity decreased in off-axis scans in controls ($P < .001$), AMD areas between drusen ($P < .001$), and AMD areas overlying drusen ($P < .001$). The magnitude of decrement in EZ reflectivity was significantly higher when incidence angles exceeded 10° in controls than in AMD areas between drusen ($P = .024$).

CONCLUSION: EZ reflectivity in dry AMD may vary by incident angle of light less than in controls, possibly indicating alteration of photoreceptor orientation or integrity.

[*Ophthalmic Surg Lasers Imaging Retina.* **2021;52:145-152.**]

INTRODUCTION

Age-related macular degeneration (AMD) is a leading cause of vision loss affecting people older than 50 years of age worldwide.[1] In its non-neovascular (dry) form, AMD is clinically characterized by drusen and extracellular lipid and protein deposits, which classically accumulate beneath the retinal pigment epithelium (RPE).[2,3] Drusen formation is associated with alteration of the RPE that, when damaged, may result in photoreceptor degeneration.[2,4-6]

Optical coherence tomography (OCT) noninvasively images retinal structure using reflectivity and interferometry.[7,8] Reflectivity of photoreceptor-associated layers including the ellipsoid zone (EZ) and the interdigitation zone (IZ) is dependent on beam entry position.[9] By purposefully shifting the OCT scanning beam to multiple pupil-entry positions and comparing the resulting images, directional OCT (D-OCT) utilizes commercial instrumentation to visualize directionally reflective retinal structures.[10] D-OCT studies have qualitatively described a marked directional reflectivity change in the outer retinal photoreceptor-associated bands, especially the EZ and IZ.[11,12] Accounting for directional reflectivity of the EZ is critical for the quantitative analysis of this layer as it may indicate photoreceptor health.[13-16]

When quantitatively measured in standard OCT, the EZ is less reflective overlying drusen.[17,18] Quantifying EZ directional reflectivity changes in intermediate AMD may allow disambiguation between photo-

From Oregon Health & Science University Casey Eye Institute, Portland, Oregon (BJL, SMG, YJ); Biostatistics & Design Program, Oregon Health & Science University – Portland State University School of Public Health, Portland, Oregon (AJJ); IBM Research, Melbourne, Victoria, Australia (BJA); and West Coast Retina Medical Group, San Francisco, California (HRM, RNJ).

Originally submitted July 20, 2020. Revision received November 23, 2020. Accepted for publication January 26, 2021.

Dr. Lujan has received grants and personal fees from Genentech/Roche; personal fees from RegenexBio, Lineage/BioTime/Cell Cure, Novartis, Regeneron; and non-financial support from Topcon outside the submitted work. He also has a patent issued for Directional OCT. Dr. Jia is supported by funding from an NIH grant and receives patent royalties and research support from Optovue. Dr. Antony is employed by IBM Research. The remaining authors report no relevant financial disclosures.

The authors would like to thank Amy Laird, PhD, for her statistical support.

Address correspondence to Brandon J. Lujan, MD, Oregon Health & Science University Casey Eye Institute, 3303 S Bond Ave., Building 1, 11th Floor, Portland, OR 97239; email: lujanb@ohsu.edu.

doi: 10.3928/23258160-20210302-05

TABLE 1

Subject Demographics

Parameter	Control (n = 17)	AMD (n = 20)
Female sex (% female)	12 (70.6)	8 (40.0)
Median age at screen (years w/ IQR)	61 (56,64)	71 (65.5,77)
Average EDTRS VA at Scan (± SD)	88.9 (5.6)	82.2 (6.6)
Scan apparent incline range (°)	6,20	6,16
Average apparent incline (°± SD)[A]	11.65 (3.97)	10.27 (2.80)
Average minor apparent incline (°±SD)[B]	8.36 (1.36)	8 (1.34, 11)
Median minor apparent incline (° w/ IQR)	8 (7, 10)	8 (7, 9)
Average major apparent incline (°±SD)[C]	14.67 (3.03)	12.55 (1.81)
Median major apparent incline (° w/ IQR)	14 (12,17)	12 (11,14)

Ages were calculated using baseline measures. EDTRS VA and apparent angle were calculated using the scan date analyzed. There were 11 incline scans in both the control and AMD minor apparent incline groups. There were 12 incline scans in the control and 11 in the AMD major apparent incline groups. Compared using a two-sample t-tests with Bonferroni correction, overall apparent angles did not significantly[A] differ comparing control to AMD subjects, nor did minor angles[B], nor did major angles[C].

EDTRS = Early Treatment Diabetic Retinopathy Study; VA = visual acuity; IQR = interquartile range; SD = standard deviation; AMD = age-related macular degeneration

receptor loss and photoreceptor misalignment. In this study, we measured EZ reflectivity in cross-sectional B-scans acquired using D-OCT in eyes with dry AMD and in controls. We hypothesize that not only is EZ reflectivity decreased in dry AMD, but also that its directional reflectivity is diminished.

PATIENTS AND METHODS

We reviewed data acquired under an institutional review board (IRB)-approved natural history imaging study in which written informed consent was obtained from all subjects. The IRB of OHSU determined that the retrospective analysis of this de-identified imaging data did not require additional IRB review. All procedures followed the tenets of the Declaration of Helsinki.

Subjects were enrolled in three cohorts: control, intermediate AMD, and geographic atrophy (GA). Inclusion criteria for all participants were age of 50 years or older and clear media. Control subjects had visual acuity (VA) no worse than 20/32 and did not have any identifiable retinal pathology in the study eye. Dry AMD subjects had VA no worse than 20/100 in the study eye and bilateral AMD with a diagnosis of intermediate AMD or GA with foveal sparing in the study eye. Those with intermediate AMD had multiple large, confluent drusen of area 0.5 disc areas (DA) or greater (≥ 1,061 µm diameter, standard circle 0.5 DA) with or without altered RPE pigmentation. GA eyes were those with well-demarcated area of GA 1 DA or greater (2.5 mm^2), or if GA was multifocal, at least one focal lesion 0.5 DA or greater (1.25 mm^2), and the largest lesion 5 DA or smaller (12.5 mm^2) residing completely within the OCT imaging field. Exclusion criteria for each group were any condition preventing central fixation, high myopia, history of other macular disease, or concurrent enrollment in an investigational treatment trial.

Eyes were dilated using 2.5% phenylephrine and 1% tropicamide. Imaging was performed according to a D-OCT protocol whereby pupil entry positions were altered to generate multiple OCT horizontal high definition 5-line raster scans with an average of 20 B-scans, each comprising 1,024 A-scans over 20° cross-sections using Cirrus 4000 HD-OCT (Carl Zeiss Meditec, Dublin, CA). At each imaging session, the primary scan was acquired via a standard centered pupil entry position yielding a visually flat scan ("flat"). Subsequently, using the integrated pupil camera, the OCT beam entry position was purposefully decentered in either direction to the largest extent possible without visibly decreasing the signal strength of the OCT image to generate visibly inclined scans ("incline"), as previously described to obtain a D-OCT set.[10,11] Previous D-OCT investigation assessing the reproducibility this imaging technique demonstrated low inter-operator, intra-operator, and inter-visit variance.[19]

Subjects were excluded from analysis if scans in the D-OCT set were not properly aligned with respect to anatomical differences in the images. All included scans were those with strong signal, and which were

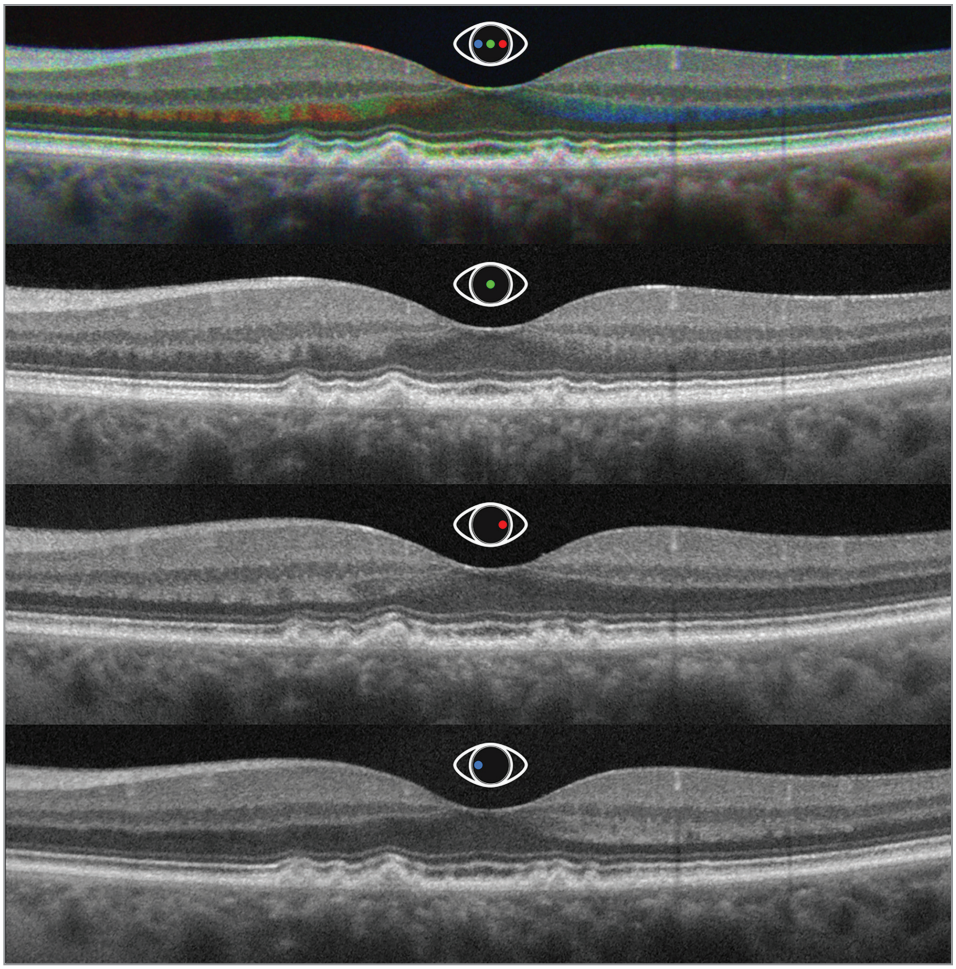

Figure 1. Aligned directional optical coherence tomography B-scans from a 58-year-old female subject with intermediate dry age-related macular degeneration. Top: chromatic image ("triposite") generated by combining colorized B-scans from all three horizontal pupil entry positions as previously described.[20] Color mapping set flat scans as green, decentered right (here temporal) scans as red, and decentered left (here nasal) scans as blue before the three channels were combined in the triposite image. Nondirectionally reflective structures show low reflectivity change via different pupil entry positions (pupil schematic), and therefore appear less colorful when the three channels are merged to create the triposite image. Overall, the ellipsoid zone is most reflective when imaged from a central pupil position and therefore appears green in the triposite image. Pupil schematics created using BioRender.com.

not significantly influenced by media opacity. In all, 17 control and 20 AMD subjects contributed well-registered horizontal B-scans to our retrospective analysis. We used data from the first available timepoint for cross-sectional analysis. Subject demographic information is provided in **Table 1**.

Proper alignment of each incline image to its corresponding flat image was achieved in a previously described manner which preserved relative axial alignment of retinal features through axial shearing by A-scan (**Figure 1**).[20]

Manual segmentation was performed by a single grader (SG) using ImageJ.[21] These were generated using the segmentation editor plugin and the segmented line tool at 2,400% to 3,200% zoom to achieve highest fidelity along the contour of the EZ in each B-scan. A custom script was written to generate a continuous string of overlapping 10 pixel × 5 pixel rectangular regions of interest (ROIs) centered on the EZ across the entire width of each B-scan totaling approximately 1,280 ROIs (one for each horizontal pixel in the 1,280 pixel × 960 pixel B-scan). Mean grey-scale pixel values were measured along with the x-coordinate of each ROI. EZ-contoured pixel value means were normalized using values specific to each scan: divided by a mean grey-scale pixel value from a 10 pixel × 5 pixel ROI within the overlying inner plexiform layer (IPL) matched by horizontal position. Accurate matching by x-coordinate was designed to account for potential optical variations within each individual A-scan, as axial alignment was preserved by the registration method employed. At the fovea, where no IPL was available for normalization, an average pixel value derived from the nearest ROIs in the parafovea was used.

Five image sets (three AMD subjects and two controls) were randomly selected for repeat segmentation by the single grader (SG) to test the repeatability of our segmentation and ROI coding methods using respectively intraclass correlation coefficient (ICC) and Cohen's kappa.

A single grader (SG) used the ImageJ angle tool to measure the degree of tilt required to register incline B-scans to their corresponding flat scans.[21]

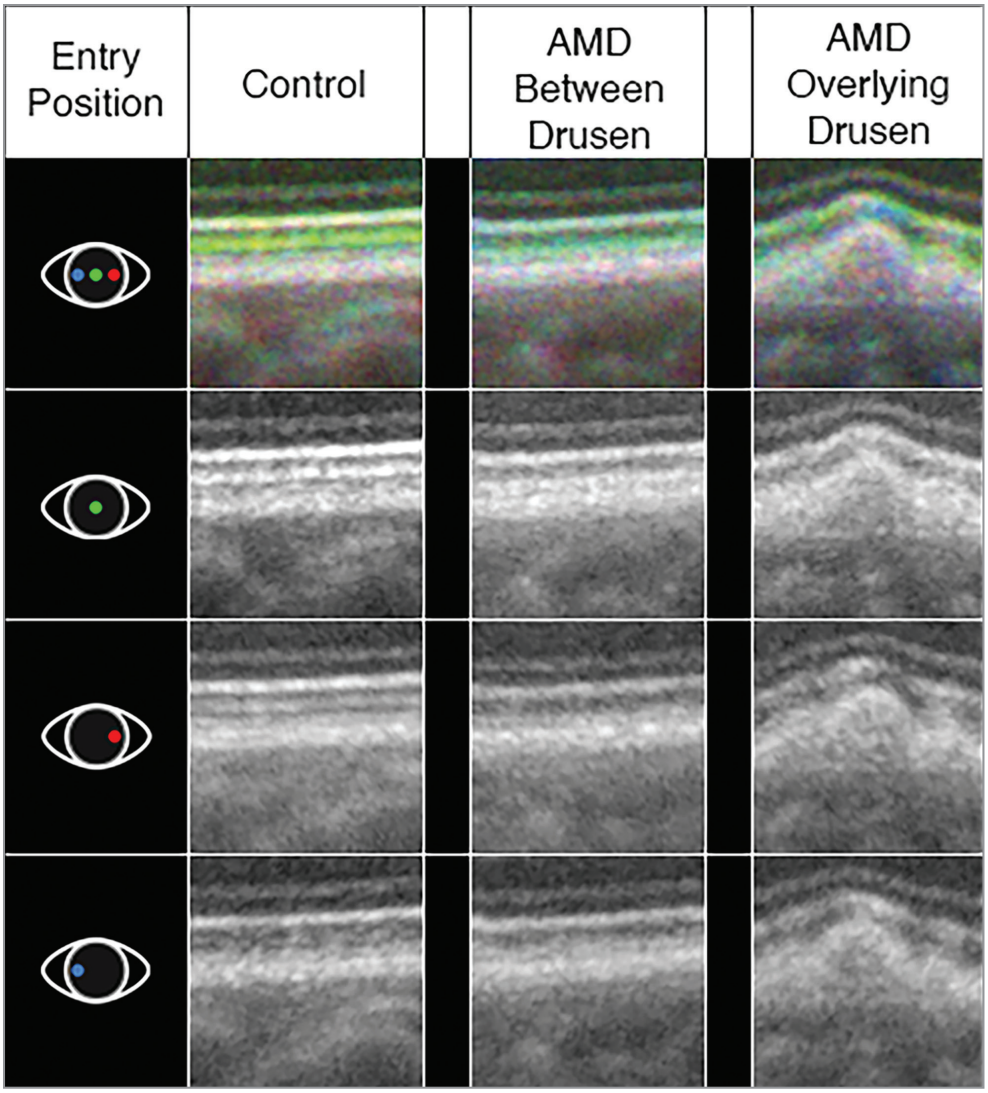

Figure 2. 100 pixel × 100 pixel area selections of registered directional optical coherence tomography B-scans from a 61-year-old female control subject and a 58-year-old female subject with intermediate dry age-related macular degeneration (AMD). Displayed sections from the control and AMD between drusen areas are approximately matched by retinal eccentricity. AMD between drusen and AMD overlying drusen 100 pixel × 100 pixel selections are sampled from identical B-scans (shown in Figure 1), allowing for comparison of the impact of pupil entry decentration on observed reflectivity of the outer retinal layers. Note the apparent absence of the interdigitation zone band in AMD overlying drusen. Pupil schematics created using BioRender.com

We then coded each individual ROI. Codes were defined as follows: exclude, between drusen, or overlying drusen. ROIs in positions with prominent blood vessels in the inner retina were excluded, as were those ROIs within 200 pixels of the scan edge. For assignment of ROIs to the drusen category, we chose a minimum lesion size, 25 pixels in the axial dimension, causing an appreciable elevation of the EZ (**Figure 2**). All ROIs visibly altered by each druse were assigned to the drusen category. Coding of individual ROIs was performed after all segmentations had been completed by a single grader (SG), and in a randomized order, generated using the Excel (Version 16; Microsoft, Redmond, WA) random number formula.

Statistical analysis was performed in Stata (Stata Statistical Software: Release 16; StataCorp, College Station, TX). Importantly, we controlled for age in all of our analyses. Using a mixed-effects model with robust standard error calculation to conservatively account for subject-level clustering, we determined the average normalized EZ reflectivity in flat scans. We examined pairwise comparisons of mean normalized EZ reflectivity in controls, AMD subjects in areas between drusen, and AMD subjects in areas directly overlying drusen with Bonferroni correction for multiple comparisons.

Using a mixed-effects model, we investigated the influence of decentering the pupil entry position while accounting for clustering by scan. We contrasted the marginal linear predictions from this model with Bonferroni correction to determine the magnitude of change in EZ reflectivity in decentered scans. To determine the impact of varying degrees of decentration, we grouped B-scans by apparent incline into three equally distributed

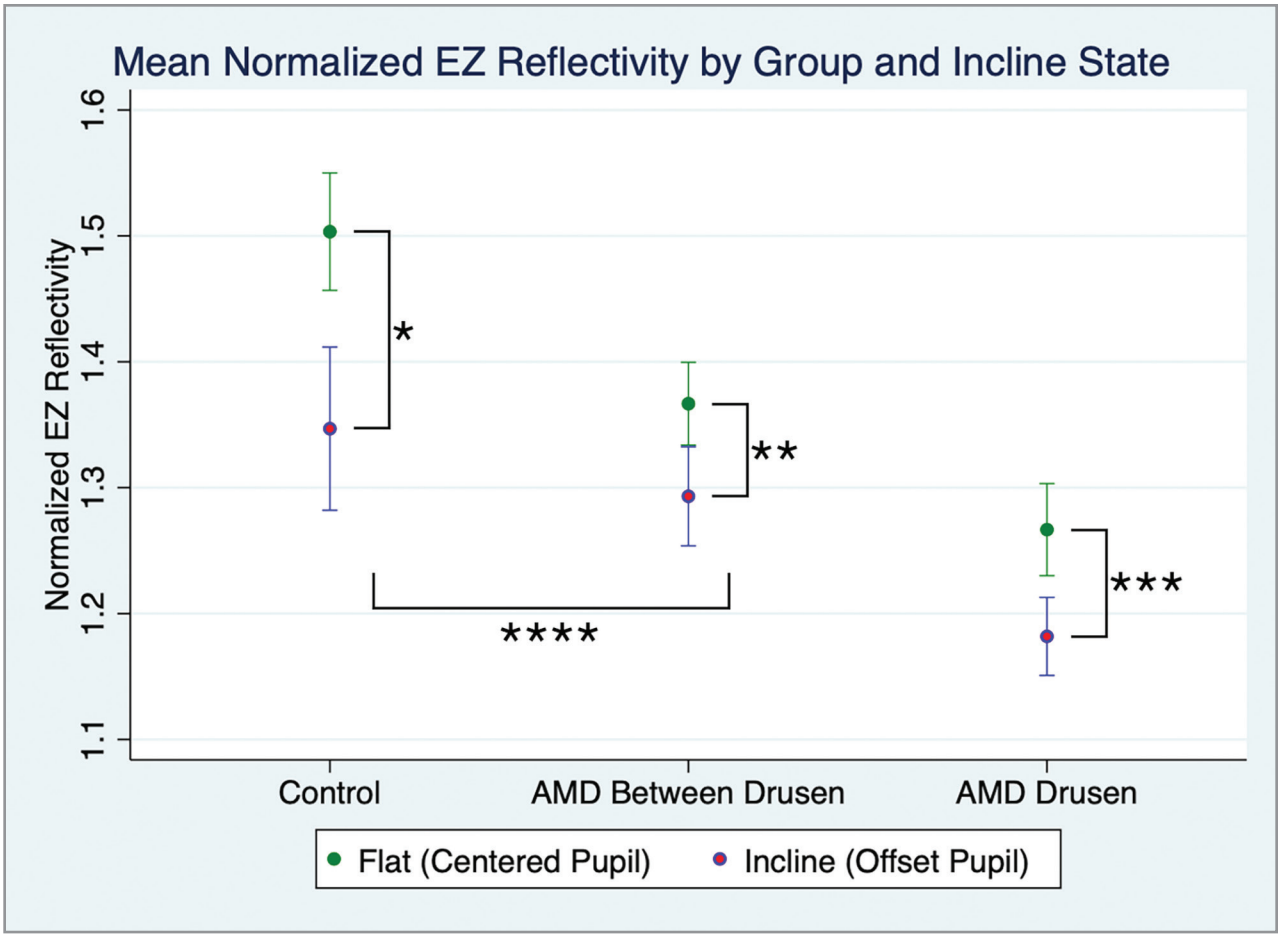

Figure 3. Average normalized ellipsoid zone (EZ) reflectivities with 95% confidence intervals are shown. A mixed-effects model accounting for clustering at the level of the subject and scan was used to compare flat scans to incline scans in controls*, age-related macular degeneration (AMD) between drusen**, and AMD overlying drusen*** and significant EZ reflectivity decrement was seen with pupil decentration in each group. A significant difference**** in magnitude of decrement was seen comparing controls to AMD between drusen.

categories: scans acquired through a centered pupil position had 0° apparent incline, decentered scans requiring 10° or less of tilt to register to their corresponding flat scan were grouped, and decentered scans requiring greater than 10° of tilt were grouped. To test whether available apparent inclines were comparable between controls and AMD subjects, we compared average incline angles using two-sample *t*-tests with Bonferroni correction. To check our assumptions, we examined the marginal and fitted residuals for each of our mixed-effects models, which were centered on zero.

RESULTS

Mean normalized EZ reflectivity was highest in flat scans in controls at 1.50 (95% confidence interval [CI], 1.46-1.55), decreased in AMD subjects in the areas between drusen at 1.37 (95% CI, 1.33-1.40), and lowest in AMD subjects overlying drusen at 1.27 (95% CI, 1.23-1.30). The difference in mean normalized EZ in flat scans between controls and AMD subjects in areas between drusen was statistically significant ($P = .005$), as was the difference in mean normalized EZ within AMD subjects comparing drusen areas to those between drusen ($P < .001$) (**Figure 3**).

Mean normalized EZ reflectivity in flat scans in the control group decreased from 1.50 (95% CI, 1.46-1.55) to 1.35 (95% CI, 1.28-1.41) in decentered scans ($P < .001$). In the AMD group between drusen, mean normalized EZ reflectivity in flat scans was 1.37 (95% CI, 1.33-1.40) and lower at 1.29 (95% CI, 1.25-1.33) in incline scans ($P < .001$). Mean normalized EZ reflectivity overlying drusen decreased from 1.27 (95% CI, 1.23-1.30) to 1.18 (95% CI, 1.15-1.21) in incline scans ($P < .001$) (**Figure 3**). There was a statistically significant difference in the magnitude of EZ reflectivity decrement in decentered scans when compar-

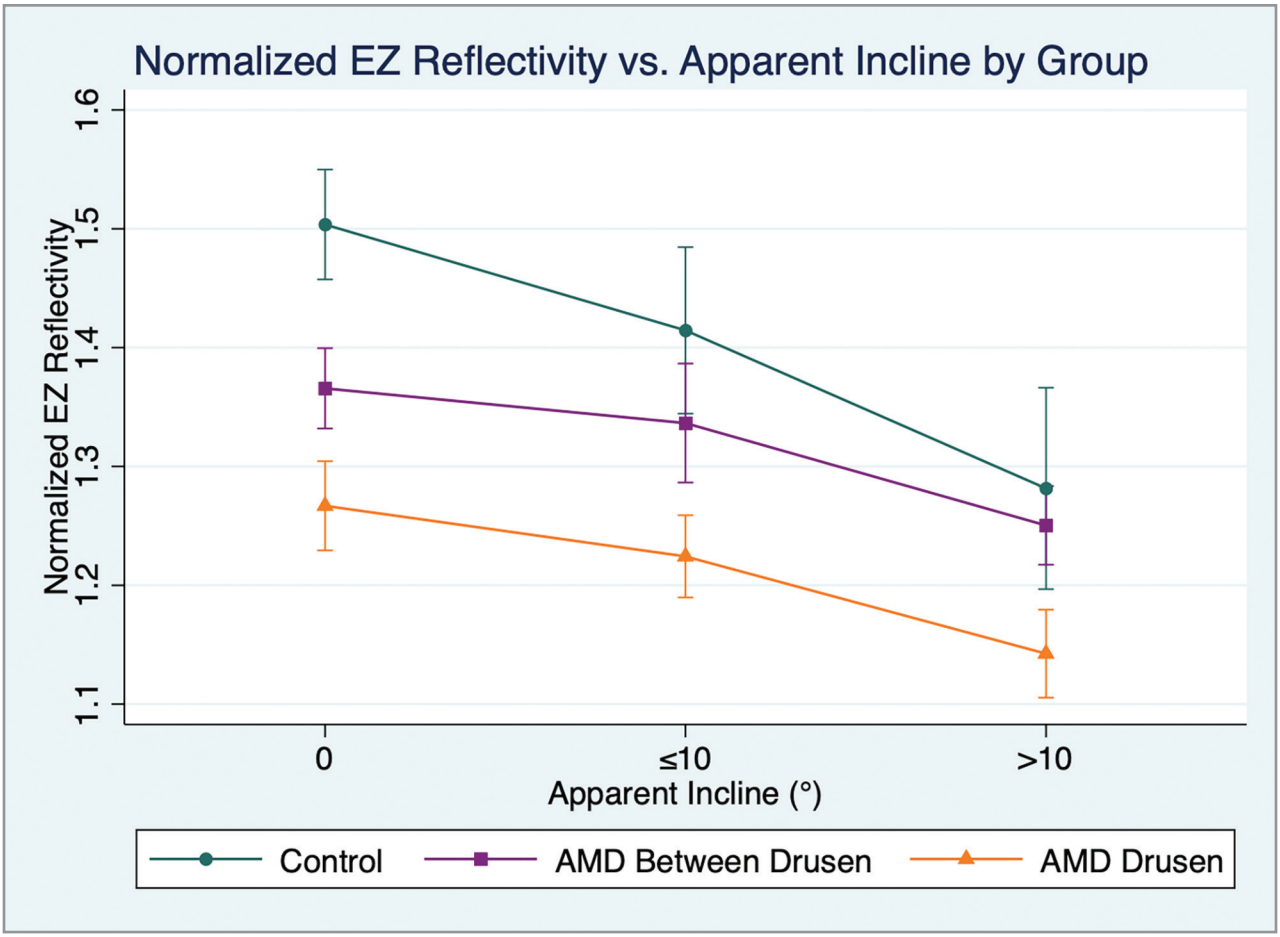

Figure 4. Mean normalized ellipsoid zone (EZ) reflectivities with 95% confidence intervals are shown. A mixed-effects model was used to contrast the marginal linear predictions across minor (≤ 10°) and major (> 10°) apparent inclines. As apparent incline is directly related to the amount of decentration in directional optical coherence tomography imaging, these groups are divided by the approximate value of 2.5-mm pupil decentration.[10,25] In all three groups, higher decrement in EZ reflectivity was seen with major than with minor decentrations. Only in controls was a significant decrease in EZ reflectivity seen with minor pupil decentration. AMD = age-related macular degeneration

ing controls to AMD areas between drusen of 0.0829 (Bonferroni-corrected 95% CI, 0.002-0.164; $P = .043$). However, the difference in magnitude of decrement comparing controls to AMD areas overlying drusen of 0.0717 (Bonferroni-corrected 95% CI, -0.014 to 0.157) was not statistically significant ($P = .119$).

Within each group, no significant differences in angles used between controls and AMD subjects existed (**Table 1**). Using Bonferroni-corrected p-values, this was evaluated by comparing average apparent incline angles ($P = .56$), average minor apparent angles ($P = 1.00$), and average major apparent angles ($P = .17$).

The decrease of -0.089 (95% CI, -0.152 to -0.026) in mean normalized EZ reflectivity with minor incline in controls was statistically significant ($P = .005$). By contrast, no statistically significant decrease in EZ reflectivity was observed with minor incline in the AMD between drusen scans ($P = .216$) nor in the AMD overlying drusen scans ($P = .070$). The magnitude of decrease with minor incline in controls did not differ significantly from -0.029 (95% CI, -0.076 to 0.017) observed in AMD between drusen (Bonferroni-corrected $P = .25$) nor from -0.043 (95% CI, -0.089 to 0.004) observed in AMD overlying drusen (Bonferroni-corrected $P = .466$). However, the decrease from flat scan mean normalized EZ reflectivity with major incline of -0.222 (95% CI, -0.300 to -0.144; $P < .001$) in controls was significantly higher than the decrease of -0.115 (95% CI, -0.142 to -0.088; $P < .001$) observed in AMD between drusen (Bonferroni-corrected $P = .024$). The decrease with major incline in controls was also higher than the decrease of -0.124 (95% CI, -0.168 to -0.080; $P < .001$) observed in AMD overlying drusen though, this difference was not statistically significant (Bonferroni-corrected $P = .068$) (**Figure 4**).

Repeatability measures demonstrated an average ICC of 0.96 (95% CI, 0.96-0.97; $P < .001$) or near perfect agreement for normalized EZ reflectivity measures obtained during two independent segmentation and normalization trials. As for repeatability of ROI coding by the categories exclude between drusen or drusen, Cohen's kappa demonstrated an 87.73% agreement between trials and a kappa score of 0.74 indicating good agreement.

DISCUSSION

Consideration of how the incident angle of light affects reflectivity is critical when quantifying pixel values of retinal layers.[16,22] Utilizing multiple OCT scanning angles, our findings demonstrate that the reflectivity of the EZ band changes in dry AMD. When imaged via a central pupil entry position, the EZ band was more reflective in control eyes than in eyes affected by dry AMD, and least reflective in areas overlying drusen. Off-axis pupil entry position reduced EZ reflectivity in controls, in AMD eyes between drusen, and in AMD eyes overlying drusen. These findings add to previous investigations in which EZ has been shown to be hyporeflective or visually discontinuous overlying drusen, hypothesized as being a result of accumulating debris disrupting wave guiding characteristics.[23,24] Our findings demonstrate that in eyes affected by drusen, the finding of a disrupted photoreceptor-associated EZ band may be due to misalignment because of its recoverable reflectivity and residual waveguiding potential.

The effects of directional reflectivity appear to be diminished in dry AMD. Only in controls was a significant decrease in normalized EZ reflectivity observed with minor apparent incline, whereas the normalized EZ reflectivity change in dry AMD was minimal. All three groups demonstrated a significant decrease with major decentration and there was a statistically significant difference in the magnitude of decrease with more major decentrations when comparing control eyes to AMD eyes in areas between drusen. These differences highlight a potential strength of directional reflectivity as a biomarker for retinal degeneration. D-OCT imaging with only minor decentrations of the pupil entry position may allow clinicians to detect alterations in expected EZ directional reflectivity due to early stages of disease and alteration of normal photoreceptor orientation.

There are several limitations to our study. Individual pupil diameters and central EZ elevation were not measured, and these may vary significantly between individual subjects. Presence of cataract, posterior capsule opacity, dry eye, refractive error, and axial length all may theoretically influence the observed reflectivity of retinal layers. However, the influence of these factors is negligible considering that our normalization technique accounted for optical variations occurring within each individual A-scan. We acknowledge that there was heterogeneity in the types of drusen analyzed and grouping them may have masked lesion-specific differences. Although we analyzed only the most accurately aligned sets of B-scans, D-OCT scans had to be acquired sequentially with scans separated by several seconds while the instrument position was being adjusted. Between subsequent acquisitions, minor changes in subject eye position may have contributed to minute variations in the anatomical position imaged within sets of D-OCT B-scans. With future instrumentation developed specifically to assess directional reflectivity, these limitations could be overcome. Although directional reflectivity may at first appear to confound the quantitative analysis of photoreceptors in AMD, these changes in optical properties may offer an additional biomarker of retinal health.

REFERENCES

1. Wong WL, Su X, Li X, et al. Global prevalence of age-related macular degeneration and disease burden projection for 2020 and 2040: a systematic review and meta-analysis. *Lancet Glob Health*. 2014;2(2):e106-e116. https://doi.org/10.1016/S2214-109X(13)70145-1 PMID:25104651
2. Khan KN, Mahroo OA, Khan RS, et al. Differentiating drusen: drusen and drusen-like appearances associated with ageing, age-related macular degeneration, inherited eye disease and other pathological processes. *Prog Retin Eye Res*. 2016;53:70-106. https://doi.org/10.1016/j.preteyeres.2016.04.008 PMID:27173377
3. Ferris FL III, Wilkinson CP, Bird A, et al; Beckman Initiative for Macular Research Classification Committee. Clinical classification of age-related macular degeneration. *Ophthalmology*. 2013;120(4):844-851. https://doi.org/10.1016/j.ophtha.2012.10.036 PMID:23332590
4. Kurihara T, Westenskow PD, Gantner ML, et al. Hypoxia-induced metabolic stress in retinal pigment epithelial cells is sufficient to induce photoreceptor degeneration. *eLife*. 2016;5:1-22. https://doi.org/10.7554/eLife.14319 PMID:26978795
5. Bhutto I, Lutty G. Understanding age-related macular degeneration (AMD): relationships between the photoreceptor/retinal pigment epithelium/Bruch's membrane/choriocapillaris complex. *Mol Aspects Med*. 2012;33(4):295-317. https://doi.org/10.1016/j.mam.2012.04.005 PMID:22542780
6. Datta S, Cano M, Ebrahimi K, Wang L, Handa JT. The impact of oxidative stress and inflammation on RPE degeneration in non-neovascular AMD. *Prog Retin Eye Res*. 2017;60:201-218. https://doi.org/10.1016/j.preteyeres.2017.03.002 PMID:28336424
7. Huang D, Swanson EA, Lin CP, et al. Optical coherence tomography. *Science*. 1991;254(5035):1178-1181. https://doi.org/10.1126/science.1957169 PMID:1957169
8. Meadway A, Sincich LC. Light reflectivity and interference in cone photoreceptors. *Biomed Opt Express*. 2019;10(12):6531-6554. https://doi.org/10.1364/BOE.10.006531 PMID:31853415
9. Gao W, Cense B, Zhang Y, Jonnal RS, Miller DT. Measuring retinal contributions to the optical Stiles-Crawford effect with optical coherence tomography. *Opt Express*. 2008;16(9):6486-6501. https://doi.org/10.1364/OE.16.006486 PMID:18516251

10. Lujan BJ, Roorda A, Knighton RW, Carroll J. Revealing Henle's fiber layer using spectral domain optical coherence tomography. *Invest Ophthalmol Vis Sci*. 2011;52(3):1486-1492. https://doi.org/10.1167/iovs.10-5946 PMID:21071737
11. Lujan BJ, Roorda A, Croskrey JA, et al. Directional Optical Coherence Tomography Provides Accurate Outer Nuclear Layer and Henle Fiber Layer Measurements. *Retina*. 2015;35(8):1511-1520. https://doi.org/10.1097/IAE.0000000000000527 PMID:25829348
12. Park DW, Lujan BJ. Normal Interdigitation Zone Loss by Motion-Tracked OCT. *Ophthalmol Retina*. 2017;1(5):394. https://doi.org/10.1016/j.oret.2017.05.005 PMID:31047567
13. Hood DC, Zhang X, Ramachandran R, et al. The inner segment/outer segment border seen on optical coherence tomography is less intense in patients with diminished cone function. *Invest Ophthalmol Vis Sci*. 2011;52(13):9703-9709. https://doi.org/10.1167/iovs.11-8650 PMID:22110066
14. Gin TJ, Wu Z, Chew SKH, Guymer RH, Luu CD. Quantitative analysis of the ellipsoid zone intensity in phenotypic variations of intermediate age-related macular degeneration. *Invest Ophthalmol Vis Sci*. 2017;58(4):2079-2086. https://doi.org/10.1167/iovs.16-20105 PMID:28388704
15. Fujita A, Aoyama Y, Tsuneyoshi S, et al. Association between visual function and the integrity of residual ellipsoid zone in resolved central serous chorioretinopathy. *Sci Rep*. 2019;9(1):12433. https://doi.org/10.1038/s41598-019-48825-7 PMID:31455795
16. Cuenca N, Ortuño-Lizarán I, Sánchez-Sáez X, et al. Interpretation of OCT and OCTA images from a histological approach: clinical and experimental implications. *Prog Retin Eye Res*. 2020;77:100828. https://doi.org/10.1016/j.preteyeres.2019.100828 PMID:31911236
17. Godara P, Siebe C, Rha J, Michaelides M, Carroll J. Assessing the photoreceptor mosaic over drusen using adaptive optics and SD-OCT. *Ophthalmic Surg Lasers Imaging*. 2010;41(6)(suppl):S104-S108. https://doi.org/10.3928/15428877-20101031-07 PMID:21117594
18. Wu Z, Ayton LN, Guymer RH, Luu CD. Second reflective band intensity in age-related macular degeneration. *Ophthalmology*. 2013;120(6):1307-8.e1. https://doi.org/10.1016/j.ophtha.2012.12.047 PMID:23732057
19. Tong KK, Lujan BJ, Zhou Y, Lin MC. Directional Optical Coherence Tomography Reveals Reliable Outer Nuclear Layer Measurements. *Optom Vis Sci*. 2016;93(7):714-719. https://doi.org/10.1097/OPX.0000000000000861 PMID:27046093
20. Makhijani VS, Roorda A, Bayabo JK, Tong KK, Rivera-Carpio CA, Lujan BJ. Chromatic visualization of reflectivity variance within hybridized directional OCT images. *Opt Coherence Tomogr Coherence Domain Opt Methods Biomed XVII*. 2013;8571:857105-1-7. https://doi.org/10.1117/12.2007141
21. Abràmoff MD, Magalhães PJ, Ram SJ. Image processing with imageJ. *Biophoton Int*. 2004;11:36-41.
22. Westheimer G. Directional sensitivity of the retina: 75 years of Stiles-Crawford effect. *Proc Biol Sci*. 2008;275(1653):2777-2786. https://doi.org/10.1098/rspb.2008.0712 PMID:18765346
23. Zayit-Soudry S, Duncan JL, Syed R, Menghini M, Roorda AJ. Cone structure imaged with adaptive optics scanning laser ophthalmoscopy in eyes with nonneovascular age-related macular degeneration. *Invest Ophthalmol Vis Sci*. 2013;54(12):7498-7509. https://doi.org/10.1167/iovs.13-12433 PMID:24135755
24. Zhang Y, Wang X, Rivero EB, et al. Photoreceptor perturbation around subretinal drusenoid deposits as revealed by adaptive optics scanning laser ophthalmoscopy. *Am J Ophthalmol*. 2014;158(3):584-96.e1. https://doi.org/10.1016/j.ajo.2014.05.038 PMID:24907433
25. Carrasco-Zevallos O, Nankivil D, Keller B, Viehland C, Lujan BJ, Izatt JA. Pupil tracking optical coherence tomography for precise control of pupil entry position. *Biomed Opt Express*. 2015;6(9):3405-3419. https://doi.org/10.1364/BOE.6.003405 PMID:26417510